LETTER TO THE EDITOR

Temperature constraints on the coldest brown dwarf known: WISE 0855-0714

J. C. Beamín[1, 2, 3], V. D. Ivanov[2], A. Bayo[4, 5], K. Mužić[2], H. M. J. Boffin[2], F. Allard[6], D. Homeier[6], D. Minniti[1, 3, 7], M. Gromadzki[3, 5], R. Kurtev[5, 3], N. Lodieu[8, 9], E. L. Martin[10], and R. A. Mendez[2, 11]

[1] Instituto de Astrofísica, Facultad de Física, Pontificia Universidad Católica de Chile, Casilla 306, Santiago 22, Chile e-mail: jcbeamin@astro.puc.cl
[2] European Southern Observatory, Ave. Alonso de Cordoba 3107, Casilla 19001, Santiago, Chile
[3] Millennium Institute of Astrophysics, Santiago, Chile
[4] Max Planck Institut für Astronomie, Königstuhl 17, 69117, Heidelberg, Germany
[5] Instituto de Física y Astronomía, Universidad de Valparaíso, Av. Gran Bretaña 1111, Playa Ancha, Casilla 5030 Valparaíso, Chile
[6] Centre de Recherche Astrophysique de Lyon, UMR 5574, CNRS, Université de Lyon, École Normale Supérieure de Lyon, 46 Allée d'Italie, F-69364 Lyon Cedex 07
[7] Departamento de Ciencias Fisicas, Universidad Andres Bello, Republica 220, Santiago, Chile
[8] Instituto de Astrofísica de Canarias (IAC), Calle Vía Láctea s/n, E-38200 La Laguna, Tenerife, Spain
[9] Departamento de Astrofísica, Universidad de La Laguna (ULL), E-38206 La Laguna, Tenerife, Spain
[10] Centro de Astrobiología (INTA-CSIC), Carretera de Ajalvir km 4, 28550 Torrejón de Ardoz, Madrid, Spain
[11] Universidad de Chile, Departamento de Astronomía, Casilla 36-D, Santiago, Chile

ABSTRACT

Context. Nearby isolated planetary mass objects are beginning to be discovered, but their individual properties are poorly constrained because their low surface temperatures and strong molecular self-absorption make them extremely faint.
Aims. We aimed to detect the near infrared emission of the coldest brown dwarf (BD) found so far, WISE0855−0714, located ∼2.2 pc away, and to improve its temperature estimate (T_{eff}= 225-260 K) from a comparison with state-of-the-art models of BD atmospheres.
Methods. We observed the field containing WISE0855-0714 with HAWK-I at the VLT in the Y band. For BDs with T_{eff} <500 K theoretical models predict strong signal (or rather less molecular absorption) in this band.
Results. WISE0855-0714 was not detected in our Y-band images, thus placing an upper limit on its brightness to Y>24.4 mag at 3-σ level, leading to Y-[4.5]>10.5. Combining this limit with previous detections and upper limits at other wavelengths, WISE0855−0714 is confirmed as the reddest BD detected, further supporting its status as the coldest known brown dwarf. We applied spectral energy distribution fitting with collections of models from two independent groups for extremely cool BD atmospheres leading to an effective temperature of T_{eff} <250 K,

Key words. (stars:) brown dwarfs – infrared: stars – stars:low-mass – stars:individual – proper motion – (Galaxy:) solar neighborhood

1. Introduction

Over the last two decades we witnessed the discovery of the first brown dwarfs (BDs; e.g., Stauffer et al. 1994; Rebolo et al. 1995; Nakajima et al. 1995; Basri et al. 1996), and a fast development of BD science, from extending the definition of stellar/substellar spectral classes to L-T-Y (Kirkpatrick et al. 1999; Martín et al. 1999; Burgasser et al. 2006; Cushing et al. 2011), to the studies of climatic variations in their atmospheres (e.g., Morales-Calderón et al. 2006; Artigau et al. 2009; Radigan et al. 2014). Within the last year we also saw how Wolf 359 (CN Leonis) was downgraded from the third to the fifth closest system to the Sun. It was surpassed by the BD binary Luhman 16AB (Luhman 2013) and by WISE J085510.83–071442.5 (hereafter WISE0855), the coldest known BD to date (Luhman 2014b).

These and other recent discoveries (Scholz 2014; Luhman & Sheppard 2014; Kirkpatrick et al. 2014; Cushing et al. 2014; Perez-Garrido et al. 2014) suggest that the census of nearby very low mass stars and BDs is still incomplete, even within a few parsecs from the Sun. The study of these ultra-cool dwarfs in the solar neighborhood and in young clusters have helped to better understand and constrain the stellar-substellar initial mass function (see Luhman 2012, and references therein), the evolution of their physical properties (Burrows et al. 2001), and the nature of their atmospheres (Biller et al. 2013).

The proximity of these new objects helps to characterize them better. For example, high quality optical spectra and optical polarimetry can be obtained despite the extremely red colors, to estimate their T_{eff}, to measure the radial velocities, and to constrain the presence of scattering disks (e.g., Kniazev et al. 2013). The higher level of brightness with respect to more distant objects makes it possible to demonstrate the spotty surface of these objects; Biller et al. (2013) and Burgasser et al. (2014) showed that the variability of Luhman 16B is related to spots and ∼30% cloud coverage; Crossfield et al. (2014) traced the clouds moving on the surface of Luhman 16B with high resolution spectroscopy and Doppler imaging. Accurate astrometry is also feasible: Boffin et al. (2014) reported indications of a planetary mass companion in the same system. Recently, Faherty et al. (2014a) confirmed the strong lithium absorption observed by

Luhman (2013) in the primary, and also detected it in the secondary component of the system (the first detection of lithium in a T dwarf) constraining the age of the system to 0.1−3.0 Gyr, revealing more details in the atmospheric and cloud properties of the system.

Luhman (2014b) discovered WISE0855 through its high proper motion (PM), 8.1±0.1 $''yr^{-1}$, by comparing multi-epoch Wide-field Infrared Survey Explorer (*WISE; Wright et al. 2010*) observations. The 4.5μm absolute magnitude indicated an effective temperature in the range T_{eff} ∼225−260 K, making it extremely faint even in the near-infrared (NIR) wavelengths, with a *J*-band upper limit of ∼23 mag. Combined *WISE* and *Spitzer Space Telescope* (Werner et al. 2004) observations yielded a parallax of 0.454±0.045 $''$(2.20$^{+0.24}_{-0.20}$ pc). Wright et al. (2014) published new NEOWISE-R (NEO WISE Reactivation mission) observations, increasing the baseline, and improving the parallax (0.448±0.033 $''$or 2.23$^{+0.17}_{-0.15}$ pc) and the PM (8.09±0.05 $''yr^{-1}$). They also reported *H*-band imaging non-detection with a limit of 22.7 mag.

Given the few positional measurements used to derive PM and parallax, and to refine its temperature estimate, we attempted to detect WISE0855 in the *Y* band. This particular band was selected based on the theoretical ultra-cool BD atmosphere models of Morley et al. (2014) that predicted weaker molecular absorption in objects with T_{eff} <300 K at λ ∼1 μm (see their Fig. 12) making them brighter in *Y* than in *J*. In Section 2 we describe our observations. In Section 3 we place an upper limit on the T_{eff} from spectral energy distribution (SED) fitting. The last section summarizes our results.

2. Observations

WISE0855 was imaged with the High Acuity Wide-field K-band Imager (HAWK-I; Pirard et al. 2004; Kissler-Patig et al. 2008) on Unit Telescope 4 of ESO's Very Large Telescope. This camera has four 2048x2048 HAWAII-2RG arrays and a plate scale of ∼0.106 $''pix^{-1}$. The target was placed on chip number 2 (as this chip shows less structure). The observations were collected on the nights of May 10 (18 images), 17 (36 images), and 28 (18 images), 2014. Each image was the average of four frames with integration of 29.2 seconds, giving a total exposure time of 140.16 minutes.

Reduction of individual frames was performed using the HAWK-I pipeline. This includes dark subtraction, division by the flat field, and sky subtraction. The files from each night were treated separately, with calibrations taken on the next day, or during the next evening twilight in the case of flats. The sky subtraction was performed in the double-pass scheme, where the first background estimate is subtracted from the science frames, which are then combined and used to create an object mask. The mask is used on the second pass to exclude the objects in the field during the creation of the final sky. Finally, the astrometric calibration of individual reduced frames was refined using bright 2MASS stars in the field as references. Two attempts of co-adding the images with SWarp v2.38.0 software (Bertin et al. 2002) were performed. First, we co-added them, leaving the reference stars fixed, to obtain a reliable detection limit on non-moving sources. The second attempt accounted for the PM of WISE0855: the images were taken with a difference in time of 17 days, implying a motion of the BD of ∼0.4$''$. We co-added the images fixing the pixels of the expected position of the moving source to obtain the photometric limit on the source of interest. The FWHM for the combined image is 0.6$''$(∼6 pixels). A zoom-
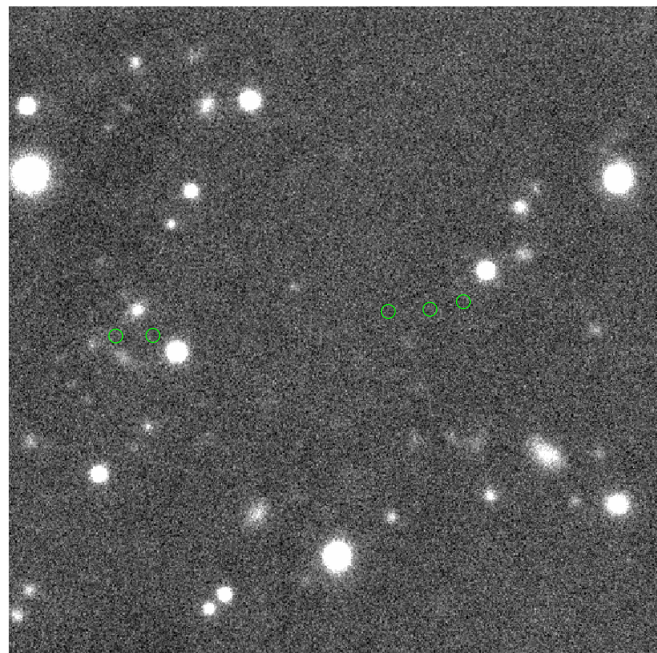

Fig. 1. A 1$'$x1$'$ field of our final *Y*-band image around the expected position of WISE0855 (north is up, east is left). Green circles mark the positions of the source given by Luhman (2014b) and Wright et al. (2014) from the *WISE* and *Spitzer* observations. The first circle on the right shows the position obtained with the WISE satellite on May 5, 2014. Our observations were made between May 10 and May 26, 2014, and the source would have moved less than 10 pixels in this image and hence would be visible at the right edge of that circle. The circle sizes are larger than the uncertainties in position.

in from this image, of the region around the WISE0855 location, is shown in Fig. 1[1].

UKIRT standards were observed each night at similar airmass as WISE0855: FS 16 on May 10, FS 136 and FS 19 on May 17, and FS 19 and FS 132 on May 28. They were reduced in the same way as the science data, and the fluxes of the standard stars were measured with large apertures (typically ∼ 5$''$) to avoid having to apply aperture corrections. The final photometric zero-point derived from these images was 26.333 ± 0.037 mag.

We performed aperture photometry with SExtractor ver. 2.19.5 (Bertin & Arnouts 1996) to both final co-added images with relaxed constraints on the detection (only five pixels above threshold and 3-σ above threshold detection, activating the algorithm to clean spurious detections). The luminosity function of the field containing WISE0855 is shown in Fig. 2. The error in the photometry as a function of the magnitude is plotted with star symbols and the vertical red line at *Y*= 24.4 shows the magnitude upper limit for WISE0855 at a 3-σ level. This limit was determined as three times the standard deviation of the sky background level around the expected position. We adopt this as our final upper limit in the forthcoming analysis. All sources detected by the software (fainter than *Y* >24.4 mag.) were removed for clarity.

3. Temperature estimates

We compare our *Y*-band upper limit of WISE0855 with the *Y*-band photometry of Y dwarfs from Leggett et al. (2013)[2]

---

[1] Figure produced with Aladin (Bonnarel et al. 2000)

[2] The HAWK-I *Y*-band filter is shifted blueward by 0.011μm compared to the UKIDSS system, and it is 0.004μm bluer compared to the NIRI
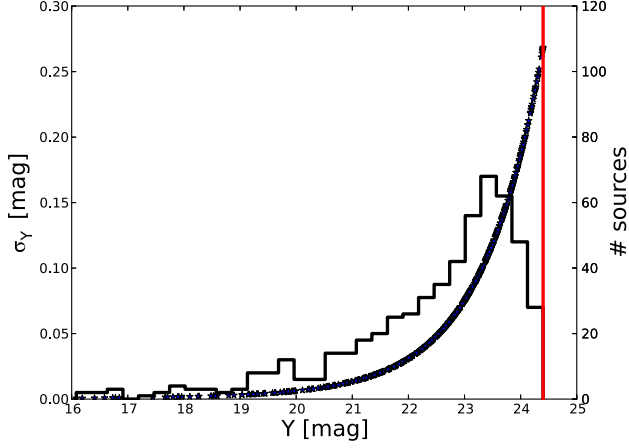
Fig. 2. Luminosity function of the sources in the field surrounding WISE0855 (black solid line) and errors on individual sources (blue stars). The red vertical line shows our detection limit at the location of the source. The photometric errors at the faint limiting magnitude are $\sim 0.25 - 0.3$ mag.
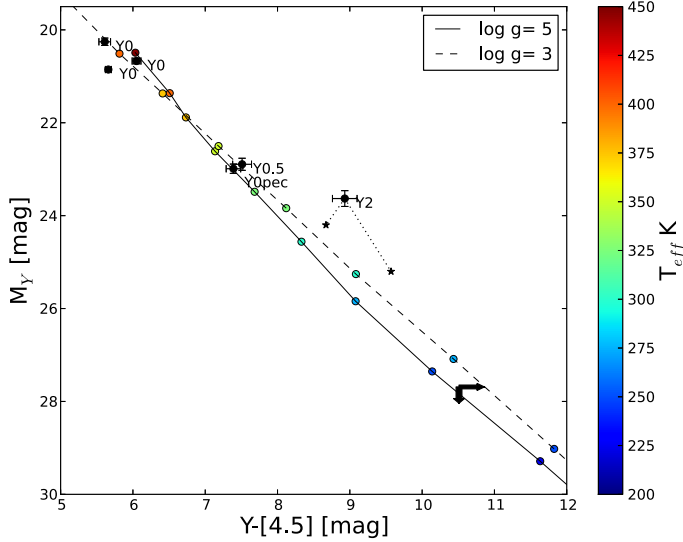

Fig. 3. Absolute color magnitude diagram of Y dwarfs with available measurements in the Y-band filter from Leggett et al. (2013). A color shift was not applied to account for differences in the pass-band from Gemini-NIRI data to VLT-HAWK-I data; distances were taken from Leggett et al. (2013) and Beichman et al. (2014). The arrow at the bottom right shows the upper limit presented in this work, making WISE0855 the reddest BD. The stars show the the individual components of the tentative Y2 binary (WISEPCJ1828+2650), proposed to explain the over-luminosity in the MIR. Colored points shows two of the models from Morley et al. (2014), with 50% cloud coverage, a sedimentation factor $f_{sed}= 5$, and log g= 3 and 5, connected with black dashed and solid line for clarity.

on a M_Y vs. Y-[4.5] CMD (Fig. 3; [4.5] measurements come from *Spitzer*). This object is $\gtrsim 1$ mag redder than the Y2

Y-band filter used in the Leggett et al. (2013) study, we decided not to transform the magnitudes to UKIDSS system and to compare directly between HAWK-I *Y*-band and NIRI *Y*-band as the filter difference between HAWK-I *Y* and UKIDSS would generate larger uncertainties. To do that, we added 0.17 mag to the values listed in table 2 of Leggett et al. (2013)
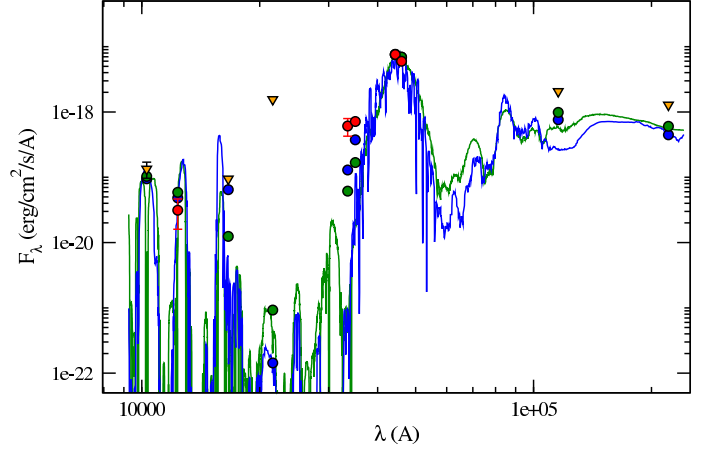

Fig. 4. Spectral energy distribution of WISE0855. Yellow triangles show the magnitude upper limits in Y (this work) and H, K_S , W3, and W4 (Luhman 2014b; Wright et al. 2014). Red circles show measurements from J band (Faherty et al. 2014b); WISE bands W1,W2 and *Spitzer* IRAC channels 1 and 2. Blue and green points represent the magnitudes derived from convolving the synthetic spectrum with the corresponding filter transmission curves for each model. Finally, the blue curve is the best fitting BT-settl model with temperature T_{eff}= 240 K, log g=4, and radius R= 1.17 R_{Jup}, conforming to all upper limits, and the green curve is the best fitting Morley et al. (2014) model, with T_{eff}= 250 K, log g= 4, f_{sed}= 7, and 50% of cloud coverage (see Morley et al. 2014 for more details in the parameters). See Sec. 3 for detailed description of the models.

Table 1. Photometric measurements and upper limits for WISE0855.

Band	Magnitude	S/N	Flux	Ref.
			[erg s^{-1} cm^{-2} Å^{-1}]	
Y	>24.4	<3	1.012E-19	(1)
J	25.	2.6	3.129E-20	(2)
H	>22.7	<3	9.423 E-20	(4)
K_S	>18.6	<3	1.555 E-18	(3)
W1	17.819±0.327	$\gtrsim$3	6.096 E-19	(4)
W2	14.016±0.048	$\gtrsim$20	5.977 E-18	(4)
W3	$\geq$11.25	<5	2.060 E-18	(3)
W4	>9	<5	1.278 E-18	(3)
IRAC [3.6]	17.44±0.05	$\gtrsim$20	7.139 E-19	(3)
IRAC [4.5]	13.89±0.02	$\gtrsim$50	7.579 E-18	(3)

References. (1) This work; (2) Faherty et al. (2014b) ; (3) Luhman (2014b); (4) Wright et al. (2014)

type WISEPCJ1828+2650, the reddest/coldest object before WISE0855 was discovered. Measurements for colder dwarfs are not available yet, so our result only indicates that WISE0855 belongs to a later type than Y2.

Only a handful of theoretical models are publicly available in the range of extremely low temperatures, inhabited by WISE0855. The field was pioneered by the now outdated AMES-COND model grid of (Allard et al. 2001). As an example, it yields a temperature T_{eff} ~100 K and a raius of ~10 R_{Jup} (which is too large) for WISE0855.

For this study we have used an updated version of the 2014 BT-Settl grid in preparation, which adds opacities of additional condensates forming at lower temperatures including Na_2S, Cr, ZnS, and KCl, and extends the cloud model calculation to temperatures where first water ice and then ammonium hydrosulphide (NH_4SH) form. In contrast to the models of (Morley et al. 2014), which incorporate a similar set of condensates, but

model the emergent spectrum as a mixture of cloudy and cloud-free patches, these models assume a homogeneous cloud deck with a thickness controlled by the balance of upmixing, settling, and depletion in the same formalism as used by the (Allard et al. 2012, 2013) models. In particular, we tested a mini-grid of updated BT-Settl models with temperatures from 380 K down to 200 K and surface gravities in the range $\log(g) = 3.5-4.5$. These models were fed into the VOSA (Bayo et al. 2008) database to compute the synthetic photometry for all filters with available photometry or upper-limits (see Table 1). The upper limits were incorporated by adding a penalizing factor for their violation, so only fits that met all the constraints were considered. The dilution factor $M_d = (R/D)^2$, where R is the object radius and D is the distance to the object, was optimized to minimize the residuals in the brute-force fit to the detections; the radius obtained for the best model was 1.17 R_{Jup}. We also fitted the new models from Morley et al. (2014)[3]. and almost the same upper limit in temperature was found; the best fit was obtained using the following parameters: $T_{eff} = 250$ K, $\log(g) = 4$, $f_{sed} = 7$ (efficiency of sedimentation).

The $T_{eff} = 240$ K, $\log g = 4$, BT-settl model (see Fig. 4) yields the best $\chi^2 \sim 8$, although still far from an ideal fit. Lower temperatures also lead to acceptable fits, suggesting that the temperatures can easily be lower. However, it is highly unlikely that WISE0855 is warmer; none of the models with $T_{eff} > 250$ K produces an acceptable fit because of the stringent *Y*- and *J*-band constraints (see Fig. 3).

4. Discussion and conclusions

We observed WISE0855 in *Y* band with HAWK-I at the ESO VLT, integrating for ~ 2.33 hours. The source was not detected, adding to the string of upper limits in *J*, *H*, K_S, and W3 bands (Table 1; and most recently in z-band; Kopytova et al. 2014). We placed a 3-σ limit of *Y* = 24.4 mag, making WISE0855 the object with the reddest NIR to MIR colors up to date. A SED fit with state-of-the-art models of extremely cool BD atmospheres was applied to all available measurements and upper limits: $T_{eff} \sim 250$ K is the maximum temperature allowed by any of the models we tested.

We investigated whether WISE0855 might belong to any of the known young moving groups: we calculated the Galactic UVW velocities[4] for radial velocities in the range from $V_{rad} = -200$ to 200 km s^{-1}, adopting the PM and the distance from Luhman (2014b) and Wright et al. (2014). There is no V_{rad} for which the UVW would match those of any of the moving groups listed in Torres et al. (2008).

WISE0855 belongs to a new, but possibly numerous (Wright et al. 2014) group of nearby extremely cool BDs and free-floating planetary mass objects. Ongoing and future deep multi-epoch surveys such as VISTA ESO public surveys (VISTA Hemisphere survey -VHS, and VISTA Variables in the Vía Láctea -VVV) UKIDSS, Pan-STARSS, Gaia, LSST, and Euclid, among others, might help to find new members of the solar neighborhood (Burningham et al. 2011; Aller et al. 2013; Beamín et al. 2013; de Bruijne 2014; Smith et al. 2014).

References

Allard, F., Hauschildt, P. H., Alexander, D. R., Tamanai, A., & Schweitzer, A., 2001, ApJ, 556, 357
Allard, F., Homeier, D., Freytag, B., & Sharp, C. M. 2012, EAS Publications Series, 57, 3
Allard, F., Homeier, D., Freytag, B., et al. 2013, Memorie della Societa Astronomica Italiana Supplementi, 24, 128
Aller, K. M., Kraus, A. L., Liu, M. C., et al. 2013, ApJ, 773, 63
Artigau, É., Bouchard, S., Doyon, R., & Lafrenière, D. 2009, ApJ, 701, 1534
Basri, G., Marcy, G. W., & Graham, J. R. 1996, ApJ, 458, 600
Bayo, A., Rodrigo, C., Barrado Y Navascués, D., et al. 2008, A&A, 492, 277
Beamín, J. C., Minniti, D., Gromadzki, M., et al. 2013, A&A, 557, L8
Beichman, C., Gelino, C. R., Kirkpatrick, J. D., et al. 2014, ApJ, 783, 68
Bertin, E., & Arnouts, S. 1996, A&AS, 117, 393
Bertin, E., Mellier, Y., Radovich, M., et al. 2002, Astronomical Data Analysis Software and Systems XI, 281, 228
Biller, B. A., Crossfield, I. J. M., Mancini, L., et al. 2013, ApJ, 778, L10
Bonnarel, F., Fernique, P., Bienaymé, O., et al. 2000, A&AS, 143, 33
Boffin, H. M. J., Pourbaix, D., Mužić, K., et al. 2014, A&A, 561, L4
Burningham, B., Lucas, P. W., Leggett, S. K., et al. 2011, MNRAS, 414, L90
Burgasser, A. J., Geballe, T. R., Leggett, S. K., Kirkpatrick, J. D., & Golimowski, D. A. 2006, ApJ, 637, 1067
Burgasser, A. J., Gillon, M., Faherty, J. K., et al. 2014, ApJ, 785, 48
Burrows, A., Hubbard, W. B., Lunine, J. I., & Liebert, J. 2001, Reviews of Modern Physics, 73, 719
Crossfield, I. J. M., Biller, B., Schlieder, J. E., et al. 2014, Nature, 505, 654
Cushing, M. C., Kirkpatrick, J. D., Gelino, C. R., et al. 2011, ApJ, 743, 50
Cushing, M. C., Kirkpatrick, J. D., Gelino, C. R., et al. 2014, AJ, 147, 113
de Bruijne, J. H. J. 2014, arXiv:1404.3896
Faherty, J. K., Beletsky, Y., Burgasser, A. J., et al. 2014, ApJ, 790, 90
Faherty, J. K., Tinney, C. G., Skemer, A., & Monson, A. J. 2014, ApJ, 793, L16
Kissler-Patig, M., Pirard, J.-F., Casali, M., et al. 2008, A&A, 491, 941
Kirkpatrick, J. D., Reid, I. N., Liebert, J., et al. 1999, ApJ, 519, 802
Kirkpatrick, J. D., Schneider, A., Fajardo-Acosta, S., et al. 2014, ApJ, 783, 122
Kniazev, A. Y., Vaisanen, P., Mužić, K., et al. 2013, ApJ, 770, 124
Kopytova, T., Crossfield, I., Deacon, N., et al. 2014, ApJ, submitted
Leggett, S. K., Morley, C. V., Marley, M. S., et al. 2013, ApJ, 763, 130
Luhman, K. L. 2012, ARA&A, 50, 65
Luhman, K. L. 2013, ApJ, 767, L1
Luhman, K. L. 2014, ApJ, 786, L18
Luhman, K. L., & Sheppard, S. S. 2014, ApJ, 787, 126
Martín, E. L., Delfosse, X., Basri, G., et al. 1999, AJ, 118, 2466
Morales-Calderón, M., Stauffer, J. R., Kirkpatrick, J. D., et al. 2006, ApJ, 653, 1454
Morley, C. V., Marley, M. S., Fortney, J. J., Lupu, R., Saumon, D., Greene, T., & Lodders, K. 2014, ApJ, 787, 78
Nakajima, T., Oppenheimer, B. R., Kulkarni, S. R., et al. 1995, Nature, 378, 463
Perez-Garrido, A., Lodieu, N., Bejar, V. J. S., et al. 2014, arXiv:1405.5439
Pirard, J.-F., Kissler-Patig, M., Moorwood, A., et al. 2004, Proc. SPIE, 5492, 1763
Radigan, J., Lafrenière, D., Jayawardhana, R., & Artigau, E. 2014, ApJ, 793, 75
Rebolo, R., Zapatero Osorio, M. R., & Martín, E. L. 1995, Nature, 377, 129
Scholz, R.-D. 2014, A&A, 561, A113
Smith, L., Lucas, P. W., Bunce, R., et al. 2014, MNRAS, 443, 2327
Stauffer, J. R., Hamilton, D., & Probst, R. G. 1994, AJ, 108, 155
Torres, C. A. O., Quast, G. R., Melo, C. H. F., & Sterzik, M. F. 2008, Handbook of Star Forming Regions, Volume II, 757
Werner, M. W., Roellig, T. L., & Low, F. J. et al. 2004, ApJS, 154, 1
Wright, E. L., Eisenhardt, P. R. M., & Mainzer, A. K. et al. 2010, AJ, 140, 1868
Wright, E. L., Mainzer, A., Kirkpatrick, J. D., et al. 2014, AJ, 148, 82

---

[3] models available at `http://www.ucolick.org/~cmorley/cmorley/Models.html`
[4] Galactic UVW Calculator, created by David Rodriguez: `http://www.astro.ucla.edu/~drodrigu/UVWCalc.html`